www.icgst.com

Voltage Source Converter of Three Phase Photovoltaic Grid Connected System and Fault Analysis

B. Dhouib, H. Hadj Abdallah
CEM Lab, Department of electrical Engineering, National School of Engineering, University of sfax, BPW, 3038
dhouib.bilel@gmail.com
http://www.enis.tn

Abstract
This paper develops a multilevel structure based on the modeling and control of a Photovoltaic (PV) application connected to a three-phase grid. The DC-DC boost converter boosts the DC voltage of the PV array to the Maximum Power Point (MPP) using a Maximum Power Point Tracking (MPPT) based on the incremental conductance method. For synchronization, a three-phase inverter is necessary to connect the PV system to the grid. The control system modeling of three phase inverter was carried out under Matlab / Simulink environment using the proportional integral controllers, pulse width modulation (PWM) three-level pulse generator technique and park transformation. The Phase Locked Loop (PLL) is used to synchronize the inverter current angle with the angle of the grid voltage to reach a power factor as close to one as possible. As a final point, different types of fault condition are created, simulated and analyzed on the grid side.

Keywords: *photovoltaic (PV), Maximum power point tracking (MPPT), pulse width modulation (PWM), voltage source converter (VSC), fault analysis*

Nomenclature

I_D	The diode current (A)
V_d	The diode voltage (V)
I_{sat}	The diode saturation current (A)
V_T	The thermal voltage
T	The cell temperature (K)
K	The Boltzmann constant, equal to $1.3806\,e^{-23}$ $\left(J \cdot K^{-1}\right)$
q	The electron charge, equal to $1.6022\,e^{-19}$ (C)
Q_d	The diode quality factor
R_{sh}	The shunt resistance
R_s	The series resistance
N_{cell}	The number of series-connected cells per module
N_{ser}	The number of series-connected module per string
N_{pp}	The number of parallel strings
ϑ_{base}	The base voltage (ϑ_{rms} line-to-line).
P_{Sc}	The inductive three-phase short circuit power in (VA)
f	The frequency in (HZ)
X	The reactance in (Ω)
(X/R)	The ratio

1. Introduction
Today, the energy demand in the world is in full evolution. However, the stock of oil in our planet will soon be exhausted. The global warming of the planet today becomes more serious due to the greenhouse effect. Some emissions of these gases are due to human activity. To reduce these emissions and ensure energy security, renewable energy is enhanced in the production of electrical energy while preserving our fossil deposits (oil and gas) as long as possible with a lesser pollution and controlled.
In recent years, there has been a growing interest in PV solar energy as it is a potential source for electricity

generation with minimal environmental impact [1]. This energy is abundant, distributed through the earth, pollution free and clean and noise-free source of energy [2]-[3].

Direct exploitation of solar energy falls within three distinct technologies: one produces calories, it is solar thermal, the second is thermoelectric generators, and the third produces electricity, it is photovoltaic (PV) solar energy, which is the subject of this paper. The growing interest in photovoltaic systems requires the growth of the activities of research and development in various aspects such as Maximum Power Point Tracking (MPPT) [4], PV arrays, anti-Islanding protection, stability and reliability, the electronic interface of power quality and power. The MPPT is used to control variations on the curve current voltage of the cells. Thus the MPPT system must track the point of optimal functioning of the PV arrays. The purpose of this technique is to ensure that the system operates very close to the optimal operating point. In regards to power electronic converter interface PV array to the grid, a DC-DC boost converter and a three-phase three-level Voltage Source Converter (VSC) are a topology widely used to this day. We used Matlab/Simulink environment to model the control system of three phase inverter using the proportional integral controllers, pulse width modulation (PWM) three-level pulse generator technique and park transformation. To get the power factor as close as possible to one, we use the Phase Locked Loop to synchronize the inverter current angle with the angle of the grid voltage.

Finally, fault analyses is carried by creating a line-to-ground (LG), line-to-line (LL), double line-to-ground (LLG) fault in the network and observe the ac voltage, ac current and ac power waveforms at the grid side with and without different types of fault condition. The remainder of the paper is organized as follows: Section (2) focuses on description of the grid connected PV system. Section (3) emphasizes on PV array model. Section (4) is dedicated to the control system of PV solar systems. Section (5) presents the grid model. Section (6) provides a calculation of asymmetrical short-circuit current: Method of symmetrical components. Our results are analyzed and discussed in section (7). The main conclusions are drawn in section (8).

2. System description

The principal schematic diagram of the grid connected PV system is presented in figure 1.The PV module is usually composed of a number of solar cells with identical characteristics. Similarly, a number of PV modules are assembled and interconnected to build a PV array. The PV array generate $72.6KW$ under standard test conditions $\left(25^{\circ}C,\ \ 1000W/m^2\right)$. The voltage level of the PV array $243V$ is boosted to $400V$ via a DC-DC boost converter using MPPT based on the incremental conductance method. This dc power is converted into ac power using a three level bridge inverter. This inverter has three legs with two switches in each leg. The switching is performed by carrier-based or space-vector based pulse width modulation. The converter produces an output waveform very close to a sinusoidal wave with extremely low harmonic distortion levels. The output L_f filter is connected to remove high switching frequency components from output current of inverter [5].A delta-star step up transformer configuration is generally used in grid connected system because the third harmonic will get circulated in delta and does not enter in the grid. To produce the pulses for the three-level bridge inverter, a dq control uses a reference frame transformation abc to dq frame which transforms the grid current and grid voltage PLL into dq frame.

3. PV array model

The basic equation that describes the I-V characteristics of the PV model is given by the following equation [2]-[6]:

$$I_D = I_{sat}\left[\exp\left(V_d / V_T\right) - 1\right] \tag{1}$$

$$I = N_{pp}I_L - N_{pp}I_{sat}\left(e\left[\frac{\left(V + R_S I\left(\frac{N_{ser}}{N_{pp}}\right)\right)}{V_T N_{ser}}\right] - 1\right) - \frac{V + R_S I\left(\frac{N_{ser}}{N_{pp}}\right)}{R_{sh}\left(\frac{N_{ser}}{N_{pp}}\right)} \tag{2}$$

where:

$$V_T = \frac{N_{cell}KTQ_d}{q} \tag{3}$$

4. Control system

The system has multiple control blocks that work together to ensure maximum power extraction from the PV array and then converting it to AC power to be injected into the grid. In this section, we discuss the details of each control block in the system.

4.1. Control of DC-DC boost converter

The DC-DC boost converter boosts the DC voltage of the PV array to the MPP using an MPPT based on the incremental conductance method. This method computes the maximum power point by comparison of the incremental conductance $\left(\Delta I / \Delta V\right)$ to the array conductance $\left(I / V\right)$. When these two are the same $\left(I / V = \Delta I / \Delta V\right)$, the output voltage is the MPP voltage. The controller maintains this voltage until the irradiation changes and the process is repeated. The incremental conductance is a technique that takes advantage of the fact that the slope of the power-voltage curve is zero at the maximum power point. The slope of the power-voltage curve is positive at the left of the MPP and negative at the right of the MPP [7] as given by:

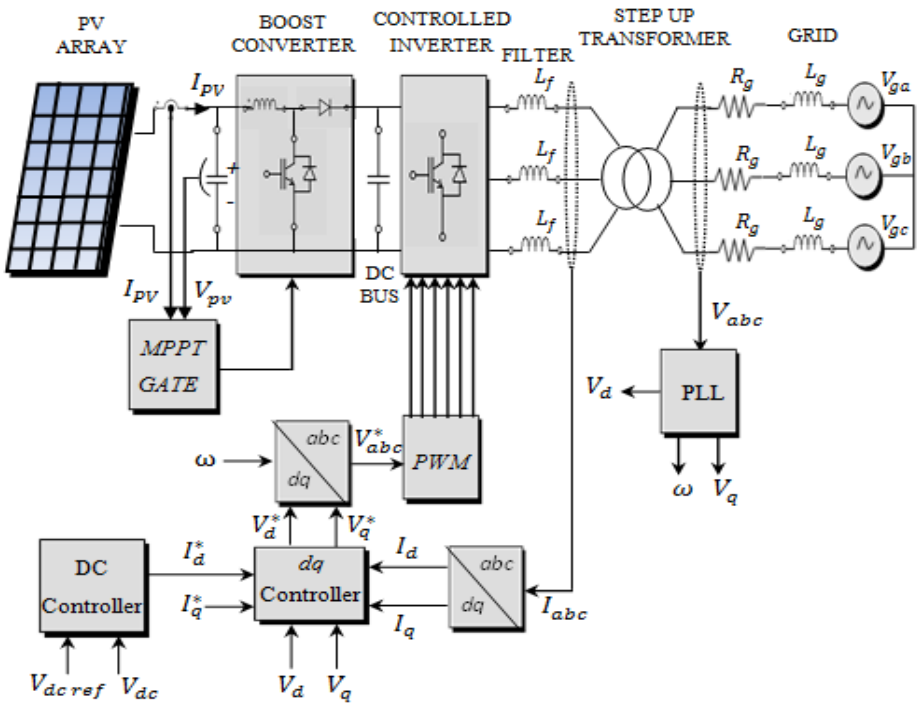

Figure 1. Schematic diagram of the grid connected PV system

$$\begin{cases} dP/dV = 0, & \text{at MPP} \\ dP/dV > 0, & \text{left of MPP} \\ dP/dV < 0, & \text{right of MPP} \end{cases} \quad (4)$$

since

$$\frac{dP}{dV} = \frac{d(IV)}{dV} = I + V\frac{dI}{dV} \cong I + V\frac{\Delta I}{\Delta V} \quad (5)$$

Therefore the equation (4) can be rewritten as:

$$\begin{cases} \Delta I/\Delta V = -I/V, & \text{at MPP} \\ \Delta I/\Delta V > -I/V, & \text{left of MPP} \\ \Delta I/\Delta V < -I/V, & \text{right of MPP} \end{cases} \quad (6)$$

We can find the MPP by comparing the instantaneous conductance (I/V) to the incremental conductance $(\Delta I/\Delta V)$ as shown in figure 2. This idea is presented in [8].

This technique has an advantage over the perturbation and observation $(P\&O)$ method because it can determine when you reach the MPP without having to oscillate around this value. It can also perform MPPT under rapidly increasing and decreasing irradiance conditions with higher accuracy than the perturbation and observation $(P\&O)$ method.

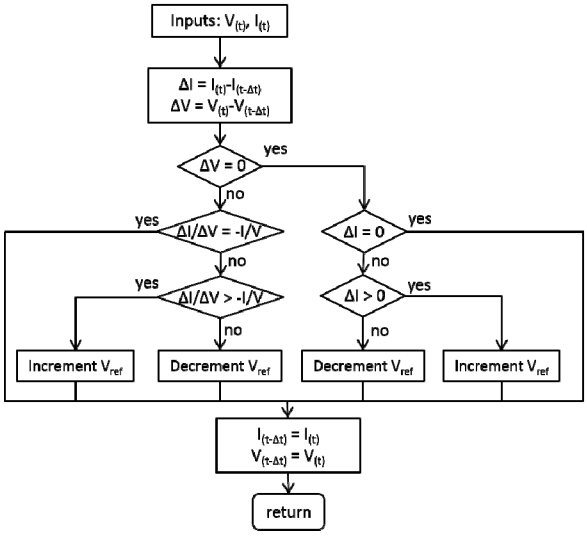

Figure 2. Flowchart for an Incremental Conductance Tracking System

4.2. Control of voltage source converter (VSC)

The three level VSC regulates DC bus voltage and keeps unity power factor. The control system uses two control loops: an external control loop which regulates DC link voltage and an internal control loop which regulates I_d and I_q grid currents (active and reactive current components). I_d current reference is the output of the DC voltage external controller. I_q current reference is set to zero in order to maintain unity power factor. V_d and V_q voltage outputs of the current controller are

converted to three modulating signals U_{ref_abc} used by the PWM three level pulse generator [9]. The determination of the grid voltage vector angle is done by a phase-locked loop (PLL) algorithm.

The grid voltage vector is used in a feed forward loop to compensate for the grid harmonics [10]. The voltage and power equations by the inverter in $d-q$ synchronous reference frame are represented below:

$$\begin{cases} V_d^* = RI_d + V_d - \omega LI_q + L\dfrac{d}{dt}I_d \\ V_q^* = RI_q + V_q - \omega LI_d + L\dfrac{d}{dt}I_q \end{cases} \quad (7)$$

$$\begin{cases} P = V_d I_d + V_q I_q \\ Q = -V_d I_q + V_q I_d \end{cases} \quad (8)$$

The voltages presented by equation (7) in the $d-q$ reference are coupled. Figure 3 shows how compensation is made for the coupling of the axes d and q. From the voltages equation by the inverter in d-q synchronous reference frame, we obtain the following decoupled voltages equation [11]:

$$\begin{cases} V_d^* = RI_d + V_d - \omega LI_q + K_p\left(I_d^* - I_d\right) + K_I\int\left(I_d^* - I_d\right)dt \\ V_q^* = RI_q + V_q + \omega LI_d + K_p\left(I_q^* - I_q\right) + K_I\int\left(I_q^* - I_q\right)dt \end{cases} \quad (9)$$

The bloc diagram is presented in figure3.

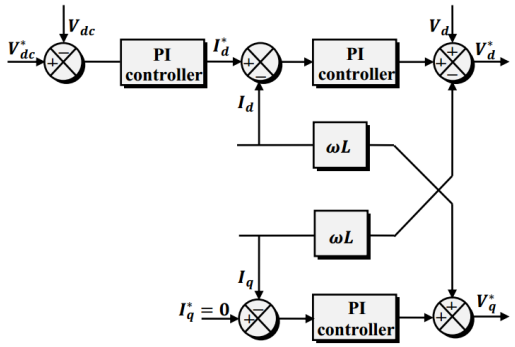

Figure 3. Compensation of the cross coupling between axes

4.3. Filter inductance L_f

To reduce the switching losses in the power components of the inverter, and aimed at improving the load current (injected current), was added an inductance [12]. The value of L_f is design based on current ripple. Typically the ripple current can be chosen as 15% - 25% of rated current. The maximum current ripple [13]-[14] can be resulting as following:

$$\Delta i_{L\max} = \frac{1}{8}\cdot\frac{V_{dc}}{L_f f_{sw}} = 20\%\cdot i_{rated} \quad (10)$$

4.4. Phase locked loop (PLL)

The PLL command is necessary in the control of the converters. Different methods to extract phase angle have been developed and presented in many papers up to now [15]-[16]. The most common method for three-phase system is that based on the representation in the referential Park of the measured voltages on the network. The principle is to consider the equations of the three-phase network in a reference Park whose orientation is such that $V_q = 0$ [17].

The phase locked loop achieves the slaving an arbitrary phase angle to the reference angle. The simulink model for a three-phase PLL is shown in figure 4.

As it can be observed, a PID controller is used in order to reduce the error between the reference and measured values of V_q. Deduce dq components from abc signals by performing an abc to $\alpha\beta$ Clarcke transformation in a fixed reference frame, then perform an $\alpha\beta$ to dq transformation in a rotating reference frame to obtain the measured value V_q.

5. Grid model

The grid was modeled as a Y connected a balanced three-phase voltage source with an internal R_g - L_g impedance [18].You can specify the source internal resistance and inductance either directly by entering R_g and L_g values or indirectly by specifying the source inductive short-circuit level and X/R ratio. The internal inductance and resistance are defined as:

$$L_g = \frac{\vartheta_{base}^2}{P_{SC}}\cdot\frac{1}{2\pi f} \quad (11)$$

$$R_g = \frac{X}{(X/R)}\cdot\frac{2\pi f L_g}{(X/R)} \quad (12)$$

6. Calculation of asymmetrical short-circuit currents: Method of symmetrical components

Any type of sinusoidal waveform (voltage, current, flux ...) can be written in terms of its symmetrical components as follows [19]:

$$\begin{bmatrix} X_a \\ X_b \\ X_c \end{bmatrix} = [F]^* \begin{bmatrix} X_1 \\ X_2 \\ X_0 \end{bmatrix} \quad (13)$$

with

$$[F] = \begin{pmatrix} 1 & 1 & 1 \\ a^2 & a & 1 \\ a & a^2 & 1 \end{pmatrix} \text{ and } \quad a = e^{j\frac{2\pi}{3}}$$

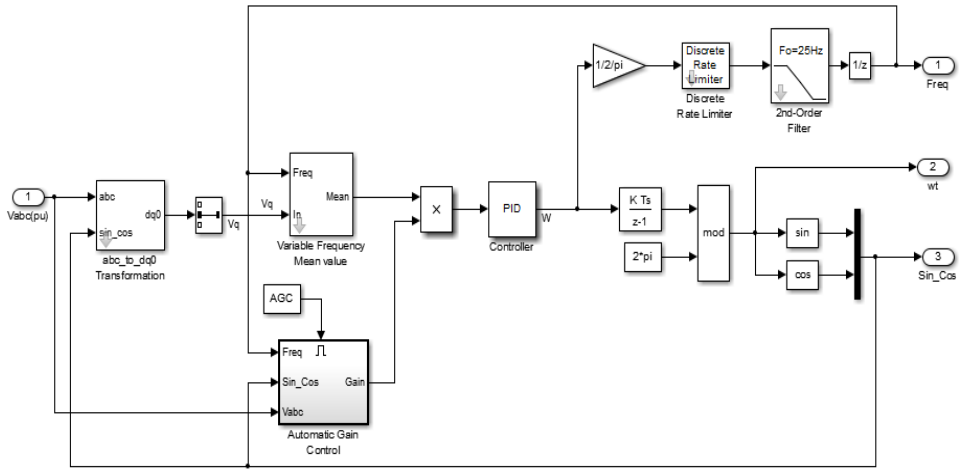

Figure 4. The Simulink model for a three-phase PLL

The sequences positive, negative and zero are determined by:

$$\begin{bmatrix} X_1 \\ X_2 \\ X_0 \end{bmatrix} = [F]^{-1} * \begin{bmatrix} X_a \\ X_b \\ X_c \end{bmatrix} \qquad (14)$$

7. Simulation results

In this section we present the simulation results of the proposed grid connected PV system presented in figure 1.

7.1. Simulation of PV system

The PV array consists of 66 strings of 5 series-connected modules connected in parallel. The total power is $(66*5*220W = 72.6KW)$. Manufacturer specifications for one module are shown in Appendix (Table 1).

Figures 5, 6, 7 and 8 shows the output characteristics of PV arrays. These curves are nonlinear and are crucially influenced by solar radiation and temperature.

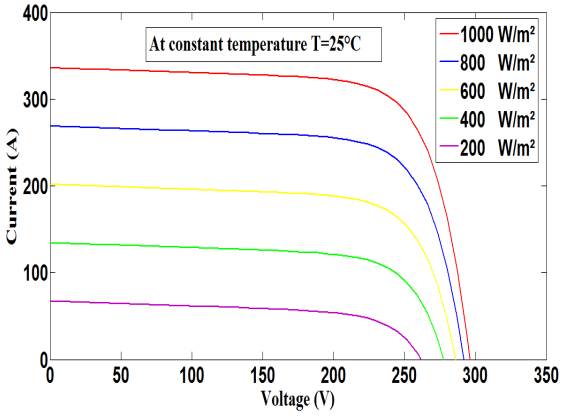

Figure 5. V-I characteristics of array under constant temperature and different irradiance

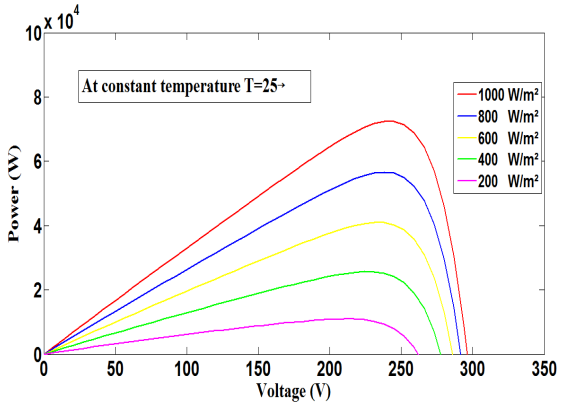

Figure 6. V-P characteristics of array under constant temperature and different irradiance

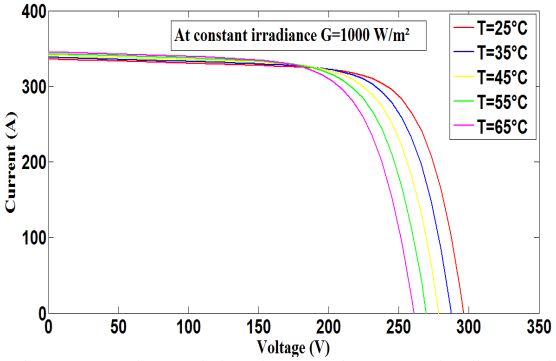

Figure 7. V-I characteristics of array under constant irradiance and different temperature

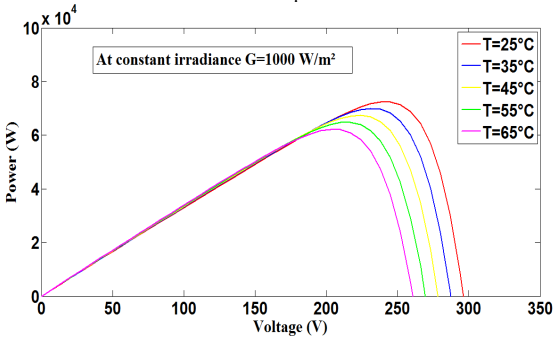

Figure 8. V-P characteristics of array under constant irradiance and different temperature

7.2. Simulation of grid connected PV system without fault

The grid connected PV system without fault in figure 1 is simulated by using MATLAB/Simulink software environment in order to validate the control methodology discussed earlier. Parameters of the test system are summarized in Appendix (Table 2).
For all simulations, the temperature is assumed constant at $25^{\circ}C$. Under steady-state condition, (i.e. constant solar irradiance $G = 1000W/m^2$), some simulation results have been chosen to illustrate the system response at standard test condition (STC).

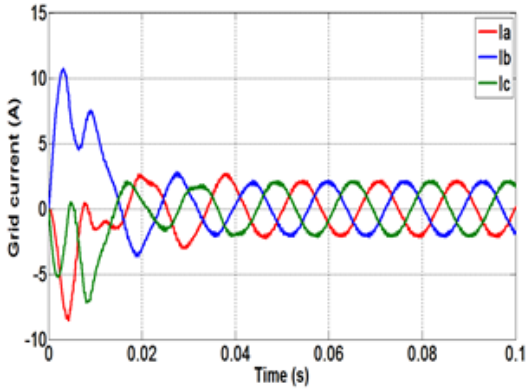

Figure 9 (a). The three phase grid current waveform

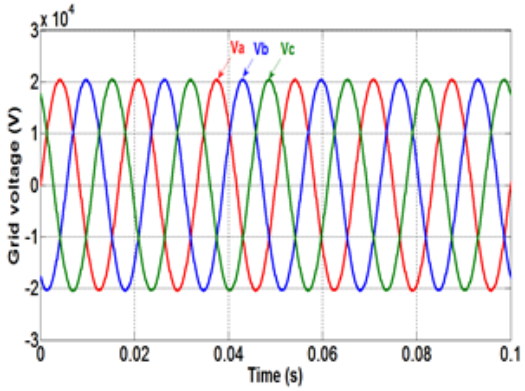

Figure 9 (b). The three phase grid voltage waveform

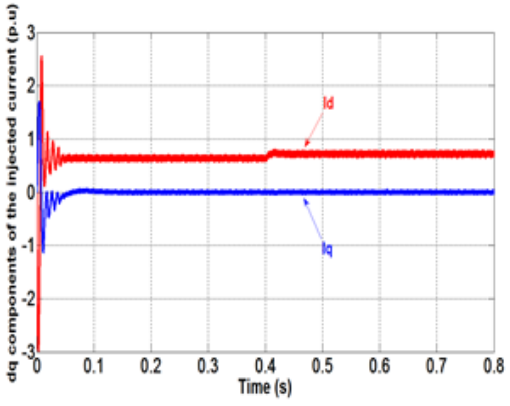

Figure 9 (c). dq components of the injected current

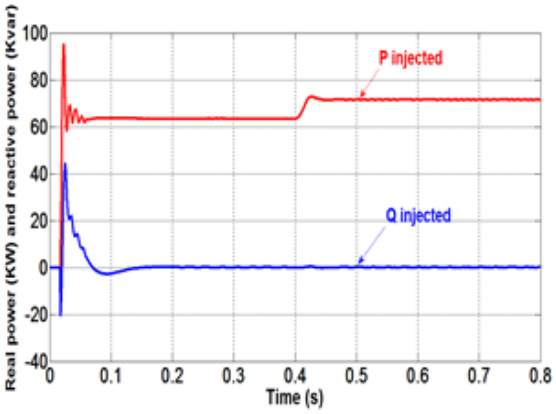

Figure 9 (d). Real power and reactive power

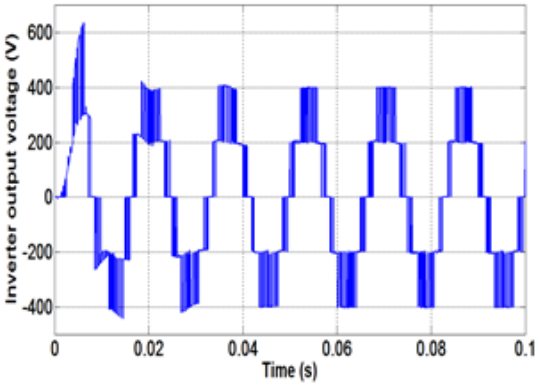

Figure 9 (e). Inverter output voltage

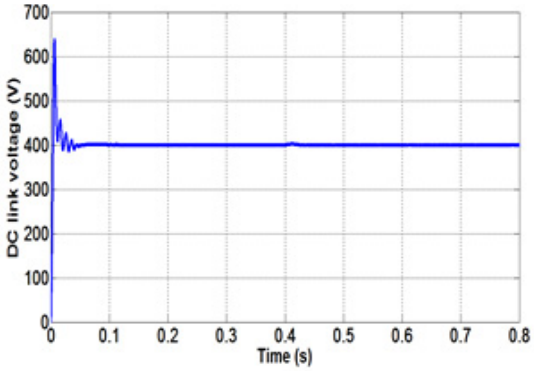

Figure 9 (f). DC link voltage

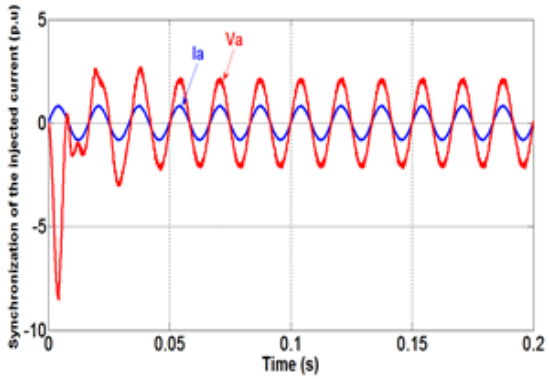

Figure 9 (g). Dynamic response of synchronization of the injected current

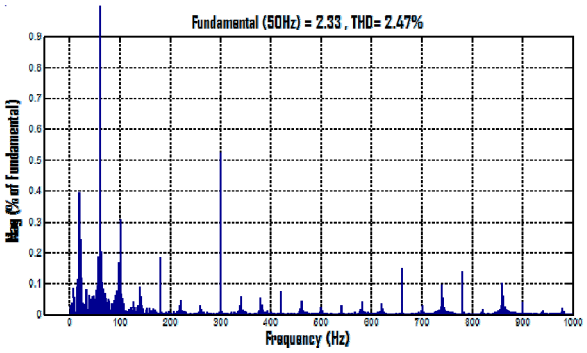

Figure 9 (h). The total harmonic current distortion in frequency domain

The three phase grid current and grid voltage waveforms are exposed in Figures 9(a) & 9(b) respectively. As can be seen, the system response under STC is very good where the steady-state conditions are reached in few AC periods. The dq components of the injected current are shown in Figure 9(c) which follow closely the references I_d^* and I_q^*. The real power and reactive power injected from the PV system are shown in Figure 9(d). The injected real power was around $71KW$ while reactive power was set to zero. To eliminate the high frequency harmonic in Figure 9(e), low-pass filter is connected. The DC link voltage was controlled at a steady state value of about $400V$ as shown in Figure 9(f). The injected currents must be synchronized with the grid voltages. So, the PLL has been used to satisfy this condition. The dynamic response of synchronization of the injected current is shown in Figure 9(g). The total harmonic distortion (THD) of the current in frequency domain is shown in Figure 9(h). The THD of current injected into the grid is 2.47% which satisfies IEEE 519 standard limits.

7.3. Effect of irradiation

In order to investigate the effectiveness of the control algorithms, a dynamic simulation is carried out with solar irradiance suddenly dropped from $1000W/m^2$ to $250W/m^2$ at 0.5sec as shown in Figure 10(a).

The effect of irradiation on PV power generation is demonstrated in figure 10. The PV array output current, voltage and power during simulation run are shown in Figures 10(b), 10(c) and 10(d) respectively. It may be noted that the effect of solar irradiance on the array terminal voltage is small compared to its effect on output current.

The simulation results of irradiation effect on PV connected to grid are illustrated in figure 11. The active and reactive powers are shown in Figure 11(a). The reactive power drops from $71KW$ to $14KW$ after $0.5\,\text{sec}$ when the reactive power is maintained equal to zero. From the simulation curve in figure 11(b), can be distinguished that the grid current amplitude decreases in response due to the sudden change of the PV generated power.

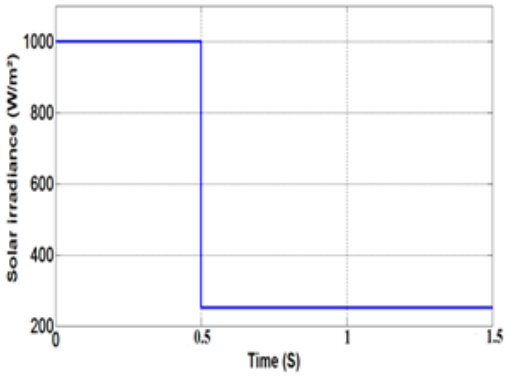

Figure 10 (a). The solar irradiance

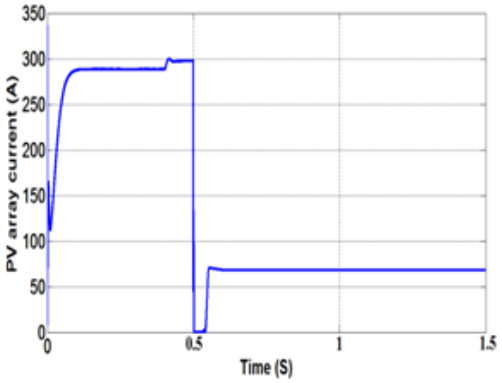

Figure 10 (b). The PV array current

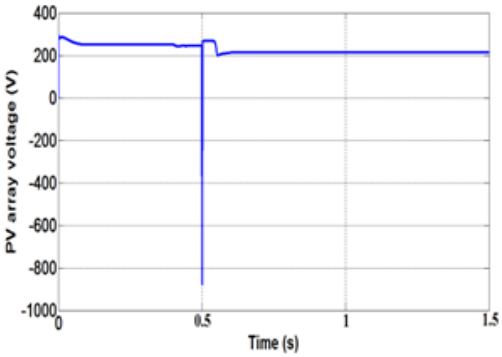

Figure 10 (c). The PV array voltage

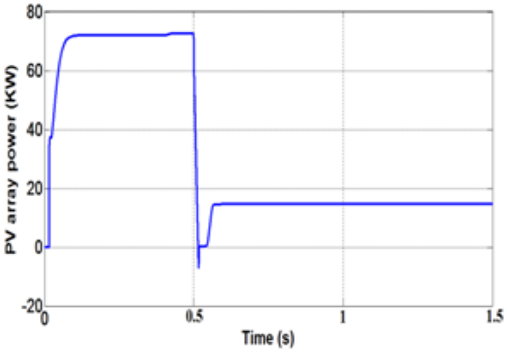

Figure 10 (d). The PV array power

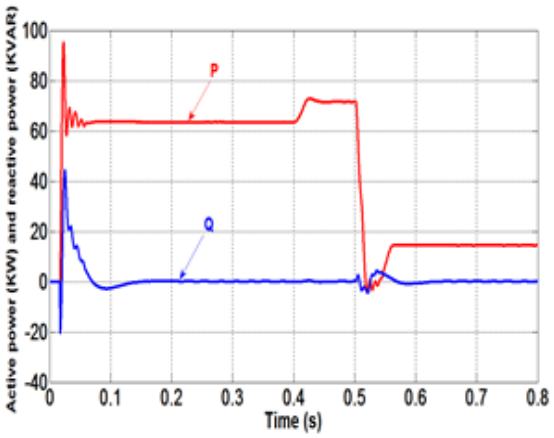

Figure 11 (a). Active and reactive power injected to the grid

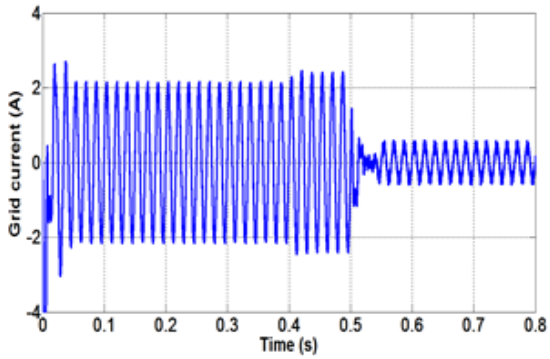

Figure 11 (b). The grid current

7.4. Simulation of grid-connected PV system with fault

The system is simulated at temperature $T = 25^{\circ}C$ and irradiance $G = 1000W / m^2$. We applying a fault on the grid side at $t = 0.55\,\text{sec}$ and the fault duration is $0.05\,\text{sec}$.

- Line-to- ground (LG) fault

Due to LG fault, the voltage V_a drops to zero as shown in figure 12. Application of fault on the grid side has resulted in oscillations in current. However, oscillations are damped as soon as the fault is cleared, and the system tracks the reference current in less than 0.2 sec. The injected current into the grid is no longer sinusoidal. This disconnection creates an increase over rated currents of the three phases currents simultaneously as shown in figure 13, this case study clearly shows an increase equal to 16.16 times of the rated current for phase A, whereas it is equal to 17.44 times for phase B and 14.24 times for phase C (see Table 3 in Appendix). In addition, this voltage failure causes a slight decrease in the level of active and reactive powers. In figure 14, the decrease of the active power is about 0.93 times of the rated power (see Table 3 in Appendix).

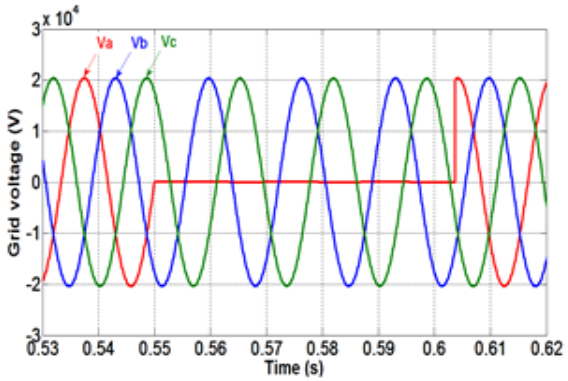

Figure 12. The grid voltage with LG fault

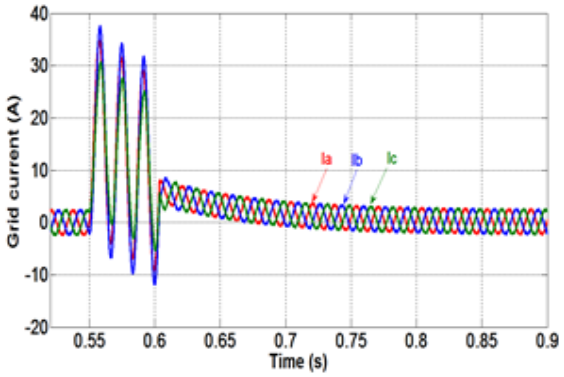

Figure 13. The grid current with LG fault

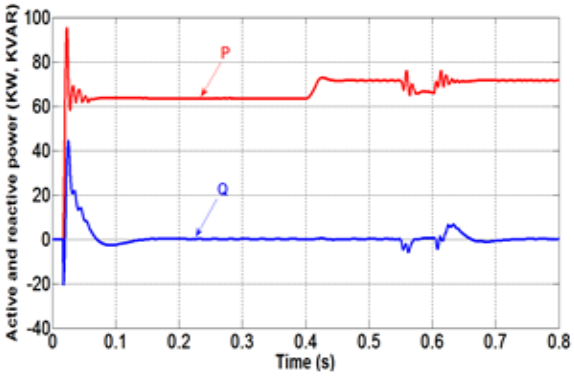

Figure 14. The active and reactive power with LG fault

- Line-to- line (LL) fault

When applying the LL fault, it can be observed from figure 15 that two phases A and B are in short-circuit during a period of fault. As a result, application of fault on the grid side has resulted in oscillations in current so that an enhances observed as shown in figure 16; this injected current into the grid is no longer sinusoidal and this boost is less important than the LG fault. For phase A, an increase of 2.17 times is reached, while for phase B an increase of 1.81 times and for phase C an increase of 2.5 times are obtained (see Table 3 in Appendix). This case study clearly shows an decrease in active power is more important for this type of fault than for the LG fault as shown in figure 17, and this decrease is 0.86 times (see Table 3 in Appendix).

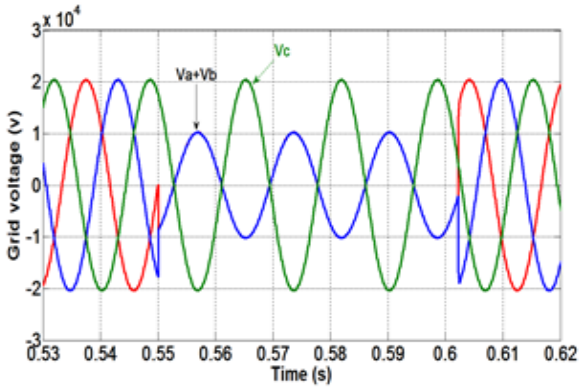

Figure 15. The grid voltage with LL fault

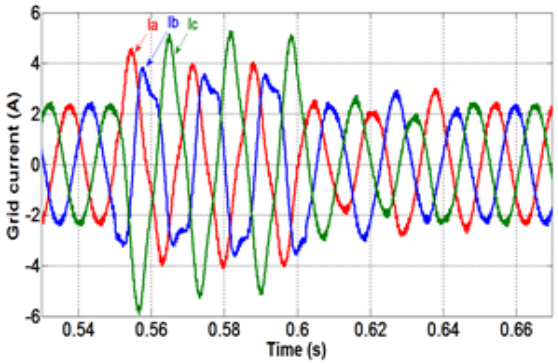

Figure 16. The grid current with LL fault

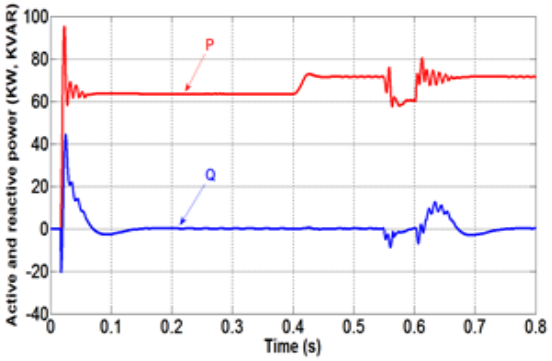

Figure 17. The active and reactive power with LL fault

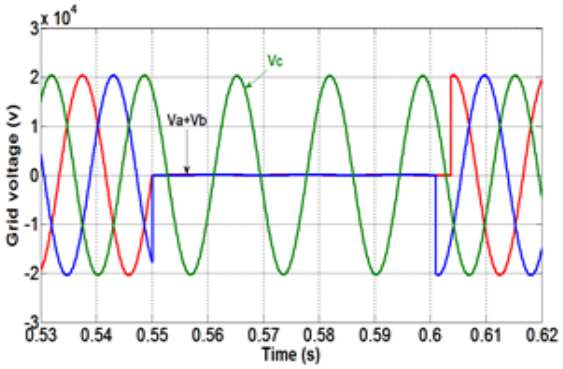

Figure 18. The grid voltage with LLG fault

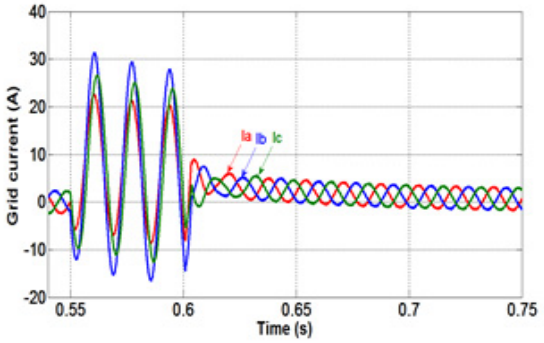

Figure 19. The grid current with LLG fault

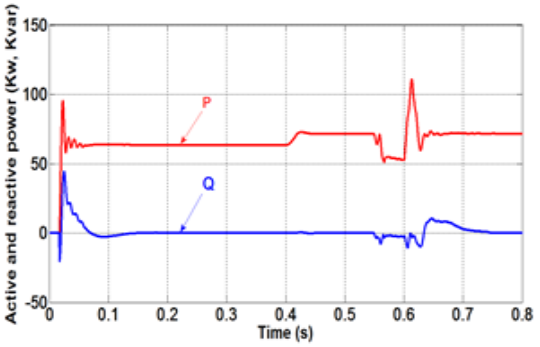

Figure 20. The active and reactive power with LLG fault

- Line-to- line to ground (LLG) fault

The different simulations of LLG fault are shown in the following figures. As shown in figure 18, phases A and B are grounded. This fault applied in the grid side causes an increase of the phase currents. However, this increase is damped as soon as the fault is cleared and the system tracks the reference current. This increase is allocated as follows: phase A- 10.72 times, phase B- 14.84 times and Phase C- 12.62 times (see Table 3 in Appendix). This increase is smaller than the LG fault but at the same time larger than the LL fault as shown in figure 19. During fault period, the active and reactive power decrease in figure 20 is less than LG and LL faults. The decrease in active power is 0.71 times (see Table 3 in Appendix).

8. Conclusion

In this paper, a grid-connected PV system based on MATLAB has been proposed. The main objectives were to achieve maximum power output from the PV array and to inject a high quality AC current into the grid.

Based on the modeling system, MPPT, steady state and dynamic performances, and fault analysis are studied. The PLL has been designed for grid synchronization and it effectively synchronizes the inverter voltage and frequency with the grid voltage and frequency. The steady state and dynamic performances of the proposed system have been tested under constant solar irradiation and fast changing solar irradiation. The presented simulation results show a good system behavior under all these case studies.

Fault analysis on grid side have been performed for various fault conditions like LG, LL, LLG faults. In case of fault, to become stable at nominal frequency, it is

observed that the system tracks the reference current in less than 0.2 sec. Application of fault on the grid side has resulted in current oscillations. The injected current into the grid is no longer sinusoidal. Disconnections create an increase over rated currents of the three phase currents simultaneously. In addition, this voltage failure causes a slight decrease in the level of active and reactive powers. The results of simulations show that the interruption due to phase to ground faults are noticeably more dangerous than the line to line faults. The decreasing of active power depends on the number of phases in fault. Nearly all PV systems will soon be required to have a fault protective device that will minimize the damages in PV arrays.

9. Appendix

- Manufacturer specifications for one module are shown in table 1

TABLE 1
ELECTRICAL CHARACTERISTIC FOR ONE MODULE

Symbol	Manufacturer	Rating values
$P_{\max}$	Maximum power	$220W$
N_{cells}	Number of series-connected cells	96
V_{OC}	Open-circuit voltage	$59.2618V$
I_{SC}	Short-circuit current	$5.09261A$
V_{mp}	Voltage at maximum power	$48.3159V$
I_{mp}	Current at maximum power	$4.54758A$

- System parameters used in simulation are shown in table 2

TABLE 2
SYSTEM PARAMETERS USED IN SIMULATION

Components	Rating value
DC link:	
Capacitance	$12000\mu F$
Reference V_{dc}	$400V$
Passive L Filter:	
Inductance: L	$250\mu H$
Resonance frequency	$50HZ$
R (in series with L)	0.002Ω
Isolation Transformer:	Step-up
Apparent power: S	$100KVA$
Primary side	$25KV \quad (L-Lrms)$
Secondary side	$230V \quad (L-Lrms)$
3 phase AC distribution grid:	
Phase-to-phase rms voltage	$25KV$
Frequency	$50HZ$
3 phase short circuit level	$100MVA$

- Phase currents and active power variations during different fault conditions are shown in table 3

TABLE 3
PHASE CURRENTS AND ACTIVE POWER VARIATIONS DURING DIFFERENT FAULT CONDITIONS

FAULT	PHASE A	PHASE B	PHASE C	ACTIVE POWER
LG	1616 %	1744 %	1424 %	93 %
LL	217 %	181.4%	250 %	86%
LLG	1072 %	1484 %	1262 %	71

10. References

[1] Hyuntae Choi, Mihai Ciobotaru. High gain DC/DC converter for the grid integration of large-scale PV systems, pp. 1011-1016, IEEE 2012.

[2] K.Manohar, P.Sobha Rani. Mppt and simulation for a Grid-Connected Photovoltaic System and Fault analysis. The International Journal of Engineering and Science (IJES) pp. 158-166, 2012.

[3] S. MALLIKA and R. SARAVANAKMAR. Closed Loop Current Control of Three Phase Photovoltaic Grid Connected System. International Journal of Electronics Communications and Electrical Engineering. Volume 5 (Issue 2) ISSN : 2277-7040, May 2015.

[4] N. Ammasai Gounden, Sabitha Ann Peter. Fuzzy logic controller with MPPT using line-commutated inverter for three-phase grid-connected photovoltaic systems, Renewable energy journal n 34. Elsevier pp. 909-915, 2009.

[5] T. Wanjekeche, D.V. Nicolae, A.A. Jimoh, Modeling and control of a cascaded NPC/H-bridge inverter with LCL filter in PV-grid application, IPEC 2010, IEEE 2010.

[6] Chih-Ming Hong, Chiung-Hsing Chen. Intelligent control of grid-connected wind-photovoltaic hybrid power systems. Electrical power & energy systems journal 55 – Elsevier pp. 554-561, 2014.

[7] Divya Teja Reddy Challa, I, Raghavendar, Implementation of Incremental Conductance MPPT with Direct Control Method Using Cuk Converter. International Journal of Modern Engineering Research (IJMER) pp-4491-4496, 2012.

[8] M. Abdelkadir, A.S. Samosir, A.H.M. Yatim and S.T. Yusuf. A New Approch of Modelling, Simulation of MPPT for Photovoltaique System in Simulink Model. ARPN Journal of Engineering and Applied Sciences Vol. 8, No. 7, July 2013.

[9] V. HimaLeela, S. Thai Subha. Control of power converter for power quality improvement in a grid connected PV system. IEEE International conference on circuits, power and computing technologies ICCPCT- pp. 26-30, 2013.

[10] Hui Zhang; Hongwei Zhou; Jing Ren; Weizeng Liu; ShaohuaRuan; YongjunGao, "Three-Phase Grid-Connected Photovoltaic System with SVPWM Current Controller," Proceedings Of IEEE 6th International Conference on Power


Electronics and Motion Control (IPEMC). pp. 2161-2164, May, 2009.

[11] Ahmed S.Khalifa and Ehab F. EI-Saadany. Control of Three Phase Grid Connected Photovoltaic Power Systems. IEEE 2010.

[12] Rihab Mahjoub Essefi, Mansour Souissi, Hsan Hadj Abdallah, Current Control Strategy for Grid Connected Photovoltaic Inverter via LCL Filter, International Review on Modelling and Simulations (IREMOS), 6 (5), pp. 1426-1434, 2013.

[13] Miss. Sangita R Nandurkar, Mrs. Mini Rajeev. Design and Simulation of three phase Inverter for grid connected Photovoltaic systems. Proceedings of Third Biennial National Conference, NCNTE, Feb 24-25, -2012.

[14] Sibasish Panda, Anup Kumar Panda and H.N Pratihari. Fault Analysis on Grid Connected MPPT based Photovoltaic System. International Journal of current Engineering and Technology Vol. 3, No. 3, August 2013

[15] P. Paramita Das, Mehrdad Kazerani, "Dynamic Modeling and Performance Analysis of a Grid-Connected Current-Source Inverter-Based Photovoltaic System" in Proc IEEE Trans. sustainable energy, vol.2, no. 4, October 2011.

[16] Ryn Marouani, Kamel Echaieb and Abdelkader Mami. Sliding Mode Controller for Buck-Boost dc-dc Converter in PV Grid-Connected System. IEEE 2012.

[17] Mihai Ciobotaru, Remus Teodorescu, Vesalius G Agelidis, Offset rejection for PLL based synchronization in grid-connected converters. Applied power electronics conference and Exposition.APEC-.23rd annual IEEE. pp. 1611-1617, 2008

[18] Riad Kadri, Jean-Paul Garbert, Member, IEEE and Gerard champenois, Member, IEEE. An Improved Maximum Power Point Tracking for Photovoltaic Grid-Connected Inverter Based on Voltage-Oriented Control. IEEE transactions on industrial electronics, vol.58, No 1, January 2011.

[19] N. Umamaheswari, P.SrinivasRaju, K.Sravanthi, K.Kalyan Kumar. Performance analysis of CSI Based PV system During LL and TPG faults. IOSR Journal of Electrical and Electronics Engineering (IOS-JEEE) pp. 101-107, 2013.

Biographies

Bilel Dhouib was born in Tunisia in 1986. He received the degree in electrical engineers in 2011, The M.S. degree in electrical conversion and renewable energies in 2012 from the National School of Engineering of Sfax-Tunisia, her research interest include study the dynamic behavior of electrical network equipped with renewable sources of energy.

Hssan Hadj Abdallah is currently professor the Department of Electrical Engineering of National School of Engineering of Sfax-Tunisia at University of Sfax and member in the '' CEMLab'' Laboratory ENIS- Sfax. He received his Mastery in electrical engineering from the superior normal school of technical teaching of Tunis-Tunisia in 1982, the diploma in-depth studies in electrical engineering from the superior normal school of technical teaching of Tunis-Tunisia in 1984, the Ph.D in electrical engineering from the superior normal school of technical teaching of Tunis-Tunisia in 1991 and Habilitation University in electrical engineering from National school of engineering of Sfax in 2007. His main research interests are electrical power system (EPS), the dispatching and the stability of the EPS, wind energy and intelligent techniques applications in the EPS. He is authors and co-authors of about 100 papers in international journals and national and international conferences.